

Distinguishing post-AGB impostors in a sample of pre-main sequence stars

Rodrigo G. Vieira¹, Jane Gregorio-Hetem¹, Annibal Hetem Jr.², Grażyna Stasińska³, and Ryszard Szczerba⁴

¹ Universidade de São Paulo, IAG - Rua do Matão, 1226, 05508-900 - São Paulo, SP, Brazil e-mail: vieira@astro.iag.usp.br

² Universidade Federal do ABC, CECs, Rua Santa Adélia, 166, 09210-170 Santo André, SP, Brazil

³ Observatoire de Meudon, LUTH, 5 Place Jules Janssen, 92190, Meudon, France

⁴ N. Copernicus Astronomical Center, Rabiańska 8, 87-100, Toruń, Poland

Preprint online version: September 13, 2021

ABSTRACT

Context. A sample of 27 sources, catalogued as pre-main sequence stars by the Pico dos Dias Survey (PDS), is analyzed to investigate a possible contamination by post-AGB stars. The far-infrared excess, due to dust present in the circumstellar envelope, is typical for both categories: young stars and objects that have already left the main sequence and are suffering a severe mass-loss.

Aims. The presence of two known post-AGB stars in our sample inspired us to seek for other *very likely* or *possible* post-AGB objects among PDS sources previously suggested to be Herbig Ae/Be stars, by revisiting the observational database of this sample.

Methods. In a comparative study with well known post-AGBs, several characteristics were evaluated: (i) parameters related to the circumstellar emission; (ii) spatial distribution to verify the background contribution from dark clouds; (iii) spectral features, and (iv) optical and infrared colors.

Results. These characteristics suggest that 7 objects of the studied sample are very likely post-AGBs, 5 are possible post-AGBs, 8 are unlikely post-AGBs, and the nature of 7 objects remains unclear.

Key words. circumstellar matter — stars: post-AGB — stars: pre-main sequence

1. Introduction

In the study of large samples of stars having unconfirmed nature, the criteria used in selection of candidates often cause sample contamination with objects of other nature than that of interest. This is the case of recurring confusion between pre-main sequence (pre-MS) stars, and post-asymptotic giant branch (post-AGB) stars. In spite of their totally different evolution, both categories of objects share common characteristics. The observed infrared (IR) excess, which originates from circumstellar dust, can be explained by re-emission of thermal radiation produced by the central source in both cases.

Instigated by the presence of two confirmed post-AGBs in a sample of possible Herbig Ae/Be (pre-MS stars of intermediate mass), we decided to analyze in detail the objects having spectral energy distribution (SED) similar to those found in evolved stars. The sample was selected from the Pico dos Dias Survey (PDS)¹ by choosing only the PDS sources showing SED more luminous in the near-IR than in the optical, which is also a known characteristic of post-AGBs.

Our goal is to distinguish, among the selected PDS sources, the *very likely*, the *possible* and the *unlikely* post-AGB objects, which could be included in “The Toruń catalogue of Galactic post-AGB and related objects”² compiled by Szczerba et al. (2007).

We first briefly describe the circumstellar characteristics of both, young stars and post-AGB objects in order to review similarities and differences that are relevant for the present work.

1.1. Pre-main sequence stars

Direct imaging is the most reliable way to study the geometry of the envelopes, and to establish input disk parameters for SED fitting models. However, sensitive imagery is constrained by several observational limits, being difficult to achieve for large samples.

In general, the circumstellar structure of pre-MS stars is traced through indirect means like spectroscopic data, for example, since the profile of spectral lines may be used to infer the physical conditions of line formation.

Short-term spectral and polarimetric variability in Herbig Ae/Be (HAeBe) stars indicate, for instance, circumstellar non-homogeneities (Beskrovnaya et al. 1995), rotation, winds (Catala et al. 1999) or magnetic field (Alecian et al. 2008). The observed SEDs of HAeBes can also be used to explain their IR excesses, which are assumed to have originated from a disk and/or an envelope surrounding the central star. Different SED shapes have been used to classify the HAeBes according to the amount of IR-excess, which is one of the diagnostics of their evolutive phase in the pre-MS.

The classification schemes of HAeBes (Hillenbrand et al. 1992, Meeus et al. 2001) are based on the SED slope in the IR band, related to the amount of IR excess and the geometric distribution of dust. However, these schemes do not consider more embedded objects, which correspond to the first phases of the young stellar objects evolution. A study of several other characteristics is required to check the pre-MS nature of the candidates, since these embedded objects have SED quite similar to those classified as post-AGB.

¹ PDS was a search for young stars based on infrared excess.

² <http://www.ncac.torun.pl/postagb2>

1.2. Post-AGB objects

Following Szczerba et al. (2007), in order to refer to the evolutionary stage after the AGB phase, we prefer to adopt the general term post-AGB instead of proto-planetary nebula, since *a priori* we have no information if our objects could become Planetary Nebulae. Post-AGB stars are luminous objects with initial mass between 0.8 and $8M_{\odot}$. They completed their evolution in the asymptotic giant branch with a severe loss of mass (10^{-7} to $10^{-4} M_{\odot}/\text{yr}$) (Winckel 2003).

When the mass-loss process has removed all the envelope around the central core, the AGB star suffers a transition from highly embedded object to a new configuration of detached envelope, being accompanied by changes in the SED shape, which acquires a double peak profile (Steffen et al. 1998). Van der Veen et al. (1989) classified a sample of post-AGBs, suggesting four classes according to the SED. Classes I to III have increasing SED slope from optical to far-IR wavelengths, while Class IV has double peak SED (maxima around near-IR and mid-IR).

Ueta et al. (2000, 2007) studied the characteristics of detached dust shells and different SED of post-AGBs by means of J-K and K-[25] colors, which respectively describe the shape of the stellar spectrum in the near-IR, and the relation between the stellar (near-IR) and dust (mid-IR) peaks. According to these authors, post-AGBs can be separated in two kinds of morphologies: elliptical (SOLE) that seem to have an optically thin shell, with starlight passing through in all directions, and bipolar (DUPLEX) that have an optically thick circumstellar torus, where the starlight passes through only along the poles. Results from the HST survey of post-AGBs presented by Siódmiak et al. (2008) support this dichotomy in the morphology of the nebulosities which was confirmed by Szczerba et al. (in preparation) for a large sample of post-AGBs. These authors found again clear differences in near-IR colors of SOLE and DUPLEX objects, which are also correlated with the SED shape: post-AGB class IV objects (double peak) are SOLE type, while class II or III (single peak) are DUPLEX.

Similar differences in SED shape are also found in pre-MS stars, indicating if the starlight is scattered in all directions (double peak SED) or not (single peak) (Hillenbrand et al. 1992, Malfait et al. 1998, Meeus et al. 2001).

The main goal of the present work is to analyze a selected sample of possible HAeBes that is contaminated by the presence of post-AGBs. As described in Sect. 2., the sample was extracted from the PDS catalogue by selecting the sources that show SED shape similar to post-AGBs. Seven characteristics, typical of evolved objects, have been used to distinguish them from the young stars in our sample. The analysis of these characteristics is presented as follows. In Sect. 3 we discuss the association with clouds in order to check (i) the effects of the interstellar medium in far-IR observed fluxes, and (ii) the occurrence of isolated objects. Spectral features and their relation with circumstellar characteristics are discussed in Sect. 4. Optical and IR colors are evaluated and compared to known post-AGBs in Sect. 5. The main results are summarized in Sect. 6, according to the criteria used to identify the most probable evolved objects, while concluding remarks and perspectives of future work are presented in Sect. 7.

2. Sample selection based on IR-excess

The Pico dos Dias Survey (PDS³) (Gregorio-Hetem et al. 1992, Torres et al. 1995, Torres 1999) was a search for young stars, based on the far-IR colors of T Tauri stars (TTs). Among the detection of more than 70 new TTs, PDS also provided a list of 108 HAeBe candidates published by Vieira et al. (2003).

Sartori et al. (2010) classified the HAeBe PDS candidates according to the SED slope (spectral index) and the contribution of circumstellar emission to the total flux. They verified that 84% of the studied PDS sources can be confidently considered as HAeBe, while the nature of several candidates remains uncertain.

In this Section we describe the criteria adopted to select the objects studied in the present work, by using spectral index and the fraction of circumstellar luminosity as tracers of IR-excess.

2.1. Spectral Index

The PDS HAeBe candidates were separated by Sartori et al. (2010) into three groups, according to the SED slope between optical and mid-IR, measured by the spectral index $\beta_1 = 0.75 \log(F_{12}/F_V) - 1$ (Torres 1999). We have selected 27 of the PDS sources of unclear nature, mainly those with high spectral index ($\beta_1 > 0.7$), which correspond to the most prominent IR excesses. For objects showing single peak SED, the spectral index is related to the level of circumstellar extinction. Even if the SED is double-peaked, high values of the β_1 index also indicate high levels of circumstellar emission (at $12 \mu\text{m}$), fairly larger than the optical flux (V band), independently of the stellar temperature.

Among the selected sources there are two previously known post-AGBs: Hen 3-1475 (PDS465) and IRAS19343+2926 (PDS581), according to evidence reported in the literature (Riera et al. 1995, Rodrigues et al. 2003, Bowers & Knapp 1989), which motivated us to study their differences and similarities when compared to other objects of the sample.

The list of the selected objects is presented in Table 1, giving their identification and the parameters used in the present work as spectral type (when available), B-V excess, IR colors (using 2MASS, AKARI and IRAS data), and equivalent width of H α line. Intrinsic polarization obtained by Rodrigues et al. (2009) is also given, when available.

2.2. Fraction of Circumstellar Luminosity

Different evolutive classes of pre-MS stars are defined according to the observed SED, which is affected by several characteristics of circumstellar envelopes like: chemistry and size distribution of grains, and inclination of the system.

The conspicuous grain features around $3.1 \mu\text{m}$ and $10 \mu\text{m}$ can be checked through *ISO* or *Spitzer* data, in order to better infer the nature of the circumstellar matter. However, due to the lack of near-IR spectral data for our whole sample⁴, disk models cannot be constrained in the present work. For this reason, we decided to adopt a simple model (Gregorio-Hetem & Hetem 2002) for the sole purpose of estimating the fraction of circumstellar luminosity. Regardless of envelope or disk parameters, we are interested in determining the integrated observed flux, in order to estimate the contribution of circumstellar flux as a fraction of the total flux, defined by $f_{\text{Sc}} = (S_{\text{total}} - S_{\text{star}})/S_{\text{total}}$.

³ PDS was conducted at the *Observatório do Pico dos Dias*, which is operated by the Laboratório Nacional de Astrofísica/MCT, Brazil

⁴ Only PDS141, 465, 518 and 581 were observed by *ISO* or *Spitzer*

Table 1. List of studied stars

PDS	2MASS	ST	E(B-V) mag	J-H mag	H-K mag	K-[25] mag	J-[18] mag	[9]-[18] mag	[12]-[25] mag	[25]-[60] mag	$W_{H\alpha}$ Å	P %
018	05534254-1024006	B7	1.42	2.17	1.68	7.41	10.26	2.04	0.42	0.10	40	–
027	07193593-1739180	B2	1.41	1.47	1.32	8.15	9.78	2.39	0.84	0.50	88	–
037	10100032-5702073	B2	1.60	1.86	1.40	8.28	10.34	2.55	1.04	1.00	105	2.76
067	13524285-6332492	B	1.56	1.59	1.49	6.23	8.56	1.51	0	-0.24	90	2.73
141	12531722-7707106	?	–	2.32	1.82	7.95	11.06	2.43	0.84	0.22	40	–
168	04305028+2300088	F0	2.14	1.74	1.19	6.51	8.53	1.87	0.19	-0.45	8	5.84
174	05065551-0321132	B3	1.01	0.76	0.65	10.38	–	–	1.17	1.95	65	–
193	05380931-0649166	B9	1.34	0.97	0.99	7.20	8.18	1.86	0.16	0.52	12	2.25
198	05385862-0716457	F0	1.13	1.03	1.01	6.95	7.60	2.79	1.70	1.07	8.5	–
204	05501389+2352177	B1	1.10	1.24	1.22	9.68	10.73	3.31	2.00	0.96	245	–
207	06071539+2957550	B?	1.20	1.18	1.21	8.20	–	–	0.62	1.77	5	–
216	06235631+1430280	B2	1.19	1.32	1.28	8.14	9.59	1.65	0.33	2.03	200	–
257	07414105-2000134	A	0.89	1.20	1.21	7.81	–	–	0.35	1.77	15	–
290	09261107-5242269	A	0.66	0.35	0.28	10.9	–	–	0.26	2.33	-7	1.74
353	12222318-6317167	B5	0.99	1.31	1.17	8.28	9.68	1.97	0.45	2.00	200	2.17
371	13473141-3639495	O9?	1.40	1.74	1.31	7.17	9.18	2.36	0.58	-0.1	40	–
394	15351712-6159041	F0	0.44	0.51	0.52	11.45	11.17	3.34	1.51	-0.7	-2	2.25
406	16050392-3945034	A5	0.40	1.08	1.05	8.33	9.19	1.95	0.79	1.94	13	3.2
431	16545918-4321496	A0	0.52	0.17	0.16	13.88	–	–	2	2.29	8	0.23
465	17451419-1756469	B	1.23	1.36	1.48	8.37	9.73	–	1.51	0.88	110	7.88
477	18003031-1647259	B1	1.37	1.43	1.19	7.42	9.08	2.22	0.41	-0.01	120	1.4
518	18273952-0349520	OB	2.30	1.74	1.35	6.85	–	–	0.37	1.53	600	3.8
520	18300616+0042336	F3	1.26	1.23	1.09	6.88	8.13	2.21	0.70	0.47	33	3.67
530	18413436+0808207	A5	0.47	1.59	1.66	7.93	9.92	2.12	0.52	-0.07	28	11.06
543	18480066+0254170	B0	1.79	0.48	0.40	8.91	8.93	3.82	1.92	0.41	0.8	1.14
551	18552297+0404353	B0	1.92	1.53	1.26	8.16	9.49	2.15	0.57	0.57	50	11
581	19361890+2932500	B1	0.89	1.98	1.72	8.58	10.82	–	1.33	0.74	200	12.22

Columns description: (1) PDS name; (2) 2MASS identification; (3) spectral type; (4) B-V excess; (5, 6, 7, 8, 9,10, 11) infrared colors; (12) $H\alpha$ equivalent width (negative values represent absorption lines); (13) intrinsic polarization.

Figure 1 shows the synthetic reproduction of observed SEDs of our sample, estimated from the blackbody emission of three components: a central star (S_{star}), a flat passive disk (S_d), surrounded by a spherical envelope (S_e). Different temperature laws are adopted: $T_d/T_{\text{star}} \propto (r_d)^{-0.75}$ for the disk (Adams & Shu 1986), and $T_e/T_{\text{star}} \propto (r_e)^{-0.4}$ for the envelope (Rowan-Robinson 1986), as used by Epchtein, Le Bertre & Lépine (1990) to reproduce the IR data of carbon stars. The observational data are from *PDS* (optical photometry), *2MASS*, *MSX*, *IRAS*, *AKARI* and *ISO* catalogues. Three curves calculated by the adopted model, without fitting purpose, illustrate the expected variation on the fraction of circumstellar luminosity. In the case of PDS465, for example, f_{sc} varies from 0.90 to 0.94, which is the typical dispersion found in our sample, leading us to adopt an error of 0.02 in the estimation of f_{sc} .

All objects of our sample have $\beta_1 > 0.7$ and $f_{\text{sc}} > 0.7$ that correspond to large amounts of circumstellar emission, suggesting two possible scenarios: they are embedded pre-MS stars or they possible are post-AGBs.

We are aware that it is important to check if the data points around $100 \mu\text{m}$ are reflecting the cloud and not the immediate vicinity of the star, due to the large *IRAS* beam size in these bands, mainly for objects lacking of *ISO* spectra or *AKARI* data, for example. In the next section we analyze the background contribution from clouds, aiming to avoid a possible contamination of interstellar matter in the far-IR data.

3. Association with dark clouds

The star formation process is typically associated with clouds, where the gravitational collapse of pre-stellar cores gives rise to the embedded protostars. Thus, the association with these clouds may be an indication of young-star nature. Unfortunately, only rough distance measurements are available for our sample

(Vieira et al. 2003), which makes uncertain the distinction between a true association from a projection effect. Due to this restriction, we decided to evaluate the *probability* of association with clouds, where the objects *apparently* closer to dark clouds *probably* have young nature (age < 2 Myr), while stars located far from clouds are expected to be evolved objects.

However, this cannot be used as a deterministic characteristic, since several examples of isolated pre-MS stars are known, as AB Aur, HD 163296, and HD100546, for example (e.g. van den Ancker 1999). Our main goals in investigating the spatial relation to dark clouds are twofold: (i) to verify the occurrence of isolated objects in our sample; and (ii) to estimate a possible far-IR background contamination.

3.1. Distance to the edge of nearest clouds

Aiming to infer the association with dark clouds, we have made use of the catalogue information compiled by Lynds (1962) and by Feitzinger & Stüwe (1984). These complementary works allowed us to find the dark clouds closer to the objects of our sample. For each dark cloud of these catalogues is assigned an *opacity class* number, which ranges from 1 to 6. We have adopted the criterion of choosing the closest dark cloud with opacity class 3 at least. This choice restricts the selected clouds to those with relevant extinction level, although it must be kept in mind that these opacity classes were defined based on visual inspection of photographic plates. Given the selection of the closest clouds, we estimated their area and distance to each star of our sample. These data have allowed us to roughly estimate the distance of our objects to the border of the selected clouds, defined by $d_{\text{edge}} = D - 0.5 \times a^{1/2}$, where D stands for the projected distance from the star to the cloud's center. By this way, a negative value for d_{edge} means that a star is found “inside” the angular region enclosed by the cloud of area a . A square area was adopted

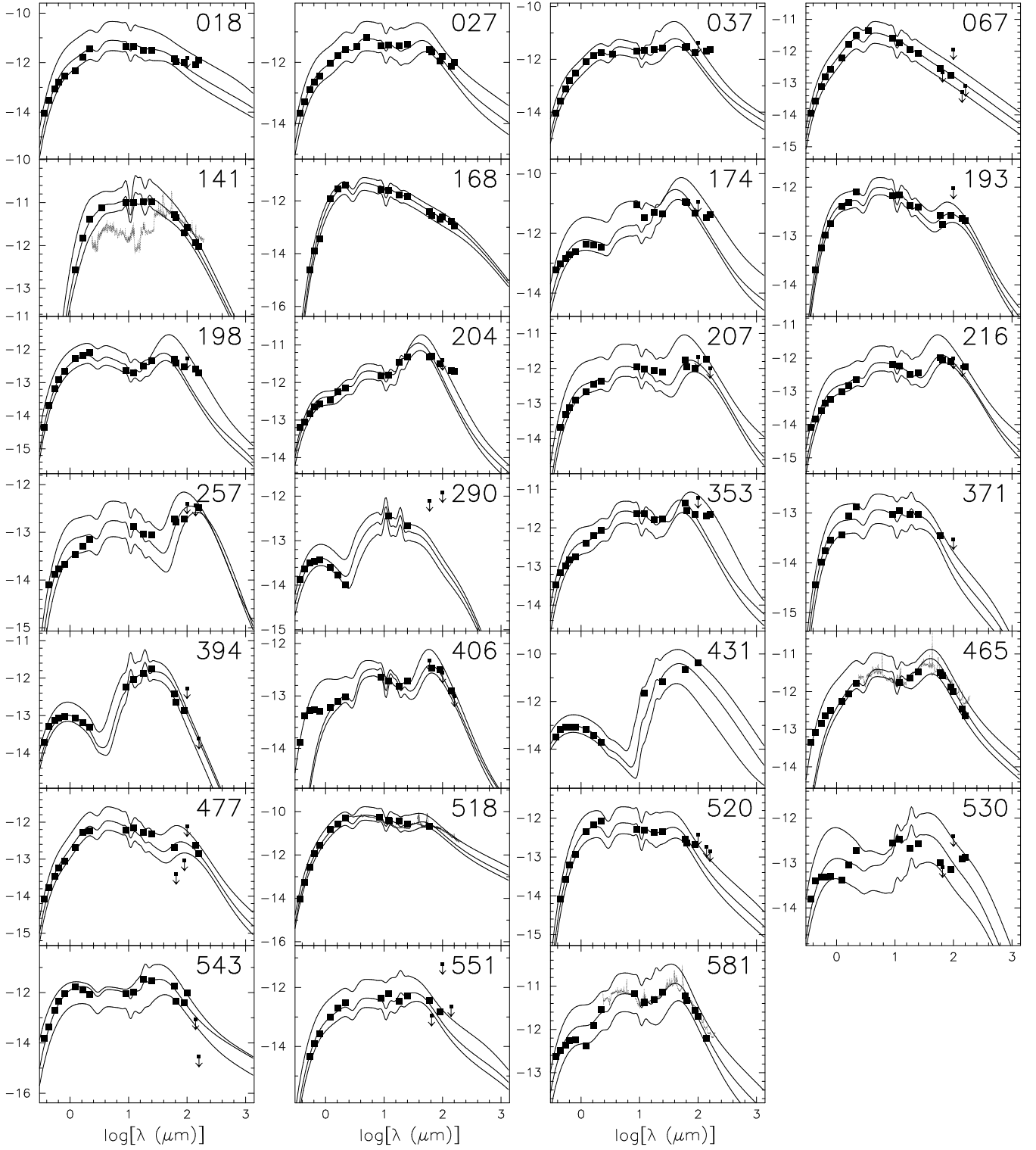


Fig. 1. Observed SED of our sample showing $\log(\lambda F_\lambda)$ in $[\text{Watt m}^{-2}]$ vs. $\log(\lambda)$ in $[\mu\text{m}]$. Filled squares represent optical photometry, 2MASS, AKARI, MSX and IRAS data, while dots are used to plot ISO spectra. Solid curves indicate the variation of the calculated SED.

in this first order calculation that does not take into account the actual shape of the cloud, which usually presents a filamentary geometry. Nevertheless, d_{edge} quantifies a possible association with the dark cloud.

3.2. Reddening

Since the information obtained from catalogues of dark clouds is related to arbitrary opacities, we adopted two other methods to evaluate dark cloud effects on the objects of our sample. First we used an extinction map, which quantifies the cloud obscuration. In the second method we estimated the color excess in order to

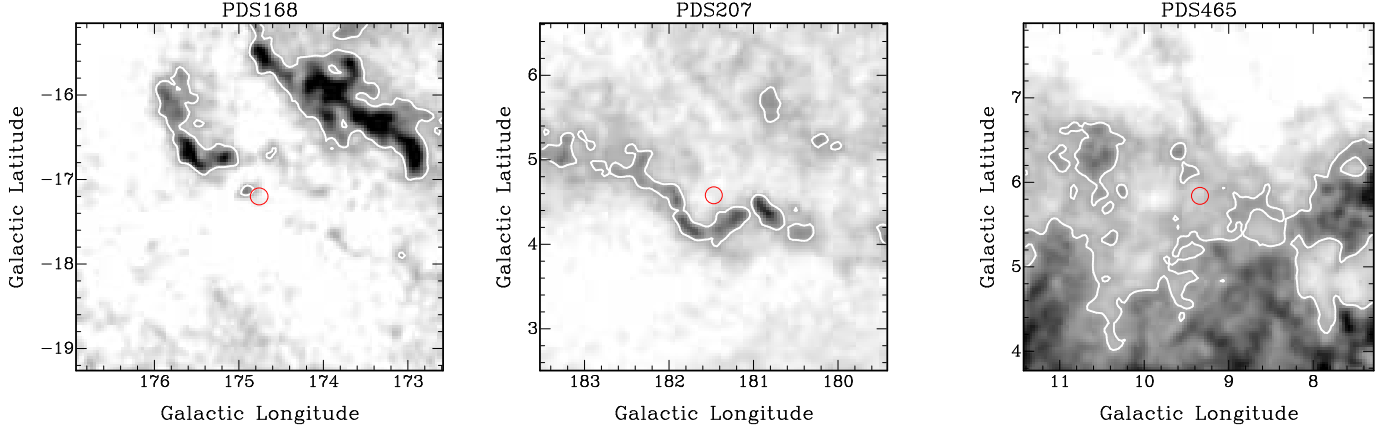


Fig. 2. Position of some of the objects (displayed by the central circle) in the Galactic extinction map produced by Dobashi et al. (2005). The half-tone grey color varies from 0 to 3 mag, while the contours show $A_V = 1.0$ mag level.

obtain the total extinction, due to both interstellar (clouds) and circumstellar (disk/envelope) extinction. These two methods are described as follows.

3.2.1. Extinction Map

We have adopted the Galactic map of visual extinction derived by Dobashi et al. (2005) using the classical star count method on the optical database of the Digitized Sky Survey I (DSS). The map⁵ provides the value of the extinction A_V for the region defined by $|b| \leq 40^\circ$. For each object, we have taken the A_V value and its mean dispersion in a neighboring region of 1 square degree, aiming to quantify the fluctuation of this extinction level in the interstellar medium. This quantity reveals the presence of a possible progenitor dark cloud behind the selected object.

The obtained extinctions and respective dispersions are given in Table 2. For illustration, some specific regions of Dobashi et al.’s map are shown in Figure 2. It must be stressed that a possible association of our objects with clouds may be due to projection effects, where the dark cloud and the star are just on the same line of sight but not physically associated. However, since we do not know the distances of our objects, we can only speak in terms of *probability* of association. Objects having low values of A_V probably are isolated, but other methods are required to confirm this information.

3.2.2. Color Excess

The visual extinction may be also estimated by means of the color excess that is caused by the absorption and scattering of the emitted light, occurring not only in the ISM but also (and sometimes predominantly) in the circumstellar environment of our sample. Aiming to estimate this total extinction, we evaluated $E(V - I)$ instead of $E(B - V)$, since the color excess on $V - I$ is less affected by the ultraviolet excess (Strom et al. 1975). The intrinsic colors were selected from Bessel et al. (1998) for different sets of effective temperature and surface gravity.

Based on the spectral type given in the *PDS* Catalogue, an estimative of effective temperatures was obtained by adopting the empirical spectral calibration provided by de Jager & Nieuwenhuijzen (1987). Considering that the luminosity

classes are uncertain for most objects of our sample, the color excess was estimated by assuming two possible classes: main sequence and supergiant that are adopted to represent H AeBes and post-AGBs respectively. Then, for each pair of luminosity class and T_{eff} we established a $\log g$ value extracted from Straizys & Kuriliene (1981), enabling the most convenient choice of intrinsic colors. The $E(V - I)$ values were converted to $E(B - V)$ by the relation derived by Schultz & Wiemer (1975): $E(B - V) = E(V - I)/(1.60 \pm 0.03)$. A normal reddening $R_V = 3.14 \pm 0.10$, which is a mean value of the interstellar extinction for several directions of the Galaxy studied by Schultz & Wiemer (1975), was adopted to estimate the total extinction that includes both ISM and circumstellar effects, given by $A_{Vtot} = 3.14 \times E(B - V)$. These are minimum values, since anomalous extinction ($R_V > 4$, for example) may be found in dense interstellar clouds (e.g. Savage & Mathis 1979). We estimate that A_{Vtot} can deviate by about 50%.

3.3. Background contribution

Far-infrared emission may also reveal the contamination by interstellar material on the observed SED. Aiming to evaluate the effects of background contamination, we have made use of *IRAS* images at $100 \mu\text{m}$, which is dominated by the ISM cirrus emission. For each *IRAS* image that contains one or more of the selected objects, we have chosen a region of 1 square degree in the neighborhood of the point sources, in order to estimate the background mean density flux and its standard deviation for each object. These background regions were selected avoiding the contamination of point sources in a radius of 1° . Table 2 gives the mean fluxes at $100 \mu\text{m}$ ($\langle F \rangle$) obtained in the background regions.

To quantify the excess of $100 \mu\text{m}$ flux we compared the flux density of the point source (F_{100}) with the mean background flux explained above, defining the fraction $f_{F100} = F_{100}/(F_{100} + \langle F \rangle)$ as an indication of flux excess. If $f_{F100} \sim 0$ the ISM dominates the local emission, while $f_{F100} \sim 1$ corresponds to an infrared excess mainly due to the circumstellar contribution.

We also evaluated the fraction of “net” visual extinction, which roughly corresponds to the optical depth of the circumstellar shell, by subtracting the interstellar obscuration (A_V) from the total extinction (A_{Vtot}). In this case, we define $f_{Av} = (A_{Vtot} - A_V)/A_{Vtot}$, where the interstellar extinction is obtained from the

⁵ Available at <http://darkclouds.u-gakugei.ac.jp>

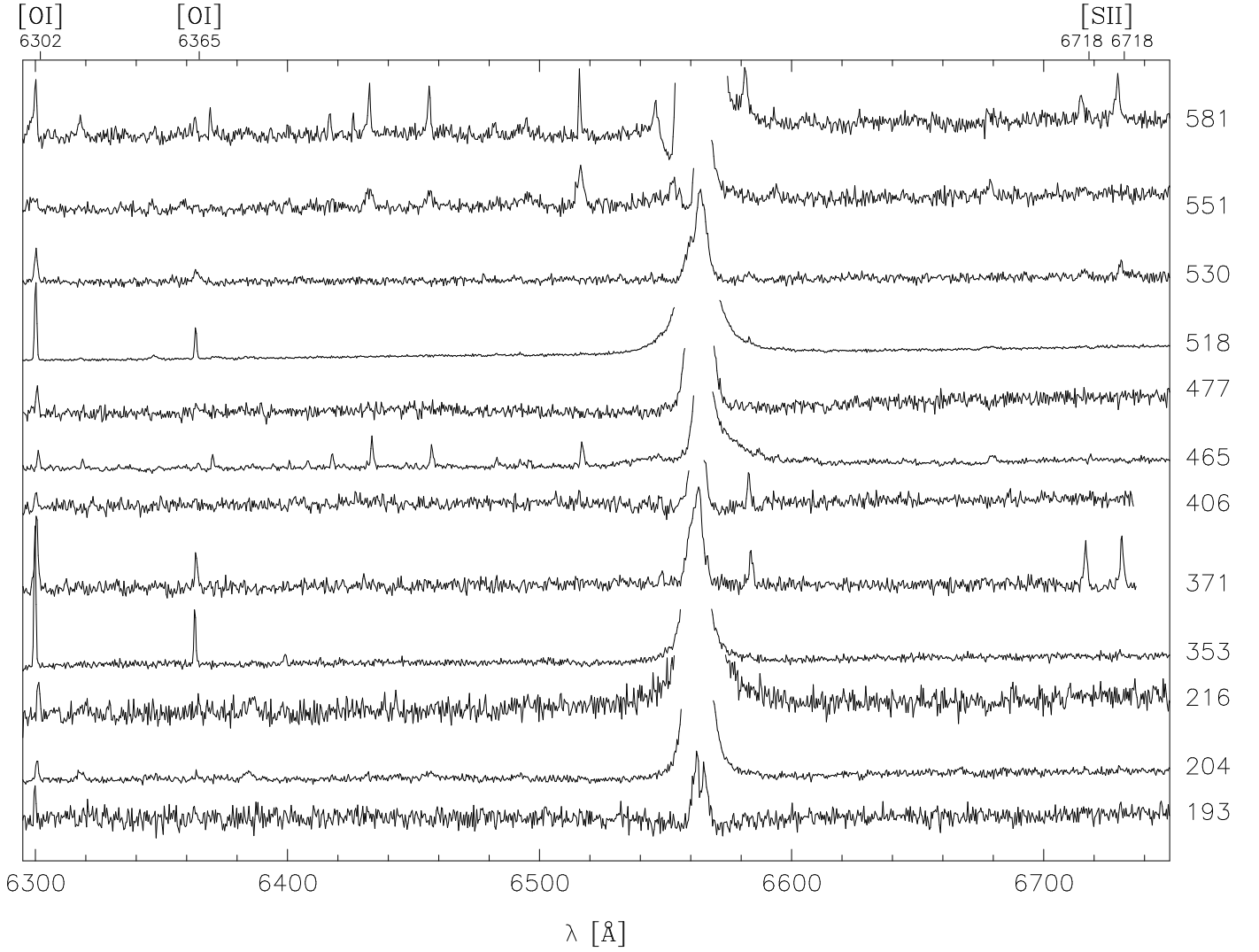


Fig. 3. Optical spectra of part of the sample, identified by the PDS number in the right side. The $H\alpha$ feature is not shown in order to enhance details of other emission lines. Intensity scale is arbitrary.

map of Dobashi et al. (2005) and the total extinction is calculated from the color excess estimated from magnitudes and spectral types given in the PDS catalogue (see Sect. 3.2.2). In this case, the effects of the adopted class of luminosity in the color excess estimation are negligible.

Table 2 shows the estimated values of f_{AV} and f_{F100} . Upper limits of f_{F100} were estimated for sources having bad quality of $100\ \mu\text{m}$ data. Excepting PDS518, all the sources with well determined f_{F100} tend to show circumstellar extinction increasing with high levels of source emission. The two known post-AGB objects of our sample have $f_{F100} > 0.5$ and $f_{AV} > 0.5$, meaning that circumstellar material has respectively prominent infrared flux and optical depth, significantly above the levels found in the corresponding background. We consider these high levels of f_{AV} and f_{F100} characteristics of post-AGBs.

4. Spectral Features

Optical spectra, obtained by the PDS team⁶, are shown in Figure 3 for the spectral regions containing [OI] (6302, 6365 Å) and

[SII] (6718, 6732 Å) nebular lines, among others. The spectra of some sources are not displayed due to different reasons: they have no emission lines, excepting $H\alpha$ (PDS174, 198, 290, 394, 520, and 543); they are too noisy (PDS168, 207, and 431); the 6300-6500 Å range was not covered (PDS18, 27, 37, 67, and 141), or the spectrum is not available (PDS257).

Almost half of our sample shows the [OI] 6302 Å emission line, but only PDS371 shows features similar to those found in evolved objects, like planetary nebulae (Pereira & Miranda 2005). Considering the absence or unclear detection of these features for the whole sample, they were not used to diagnose the nature of our objects.

The equivalent width of the $H\alpha$ line ($W_{H\alpha}$) of the objects in our sample was measured whenever possible and reported in Table 2. In the case of spectrum showing low signal-to-noise, we used the $W_{H\alpha}$ published in the PDS catalogue.

Most of the spectra show strong $H\alpha$ emission line, but two of them appear in absorption (PDS290 and 394). Line variability is a possible explanation to the weak $H\alpha$, usually seen in pre-MS stars.

A comparison of the fraction of circumstellar luminosity (f_{sc}) with the strength of $H\alpha$ line is shown in Figure 4. The distribution of objects with $W_{H\alpha} < 50\ \text{Å}$ spreads along the whole

⁶ The original files were made available by S. Vieira, on the website <http://www.fisica.ufmg.br/~svieira/TRANSF/>

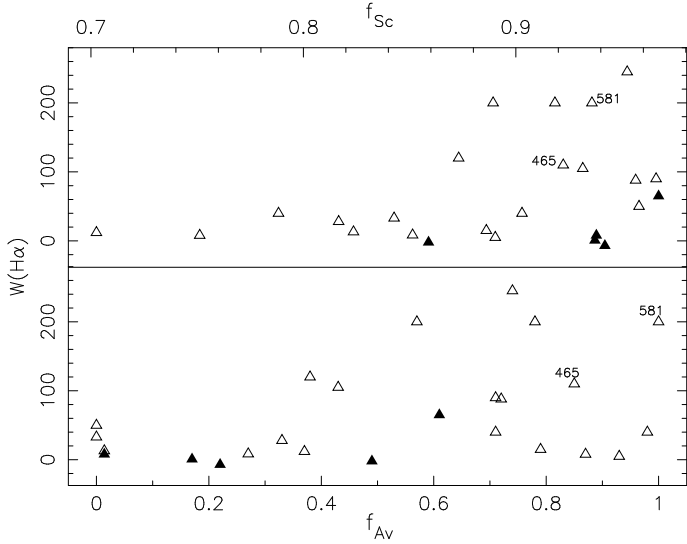


Fig. 4. Equivalent width of H_α line compared to $f_{H\alpha}$ (top) and f_{Av} (bottom) for our stars, excepting PDS518, which has $W(H_\alpha)=600 \text{ \AA}$. Filled triangles are used to show the PDS sources with double peak in the SED, while open triangles represent single peak.

range of $f_{H\alpha}$. On the other hand, objects showing strong emission line are mainly concentrated in the region of $f_{H\alpha} > 0.87$. As illustrated in Fig. 4, a similar distribution is found in the diagram of $W_{H\alpha}$ in function of f_{Av} , which is indicative of optical depth of the circumstellar shell, discussed in Sect. 3.3.

5. Analysis of color-color diagrams

To understand the nature of our objects it is necessary to carry out a multi-wavelength analysis. For this purpose, we have made use of two-color diagrams in several spectral ranges. The photometric optical data were obtained from the *PDS* catalogue. The measurements were taken in the Johnson-Cousins photometric system $UBV(RI)_c$, with the high-speed multicolor photometer (FOTRAP) described by Jablonski et al. (1994).

The catalogues *2MASS*, *IRAS*, *MSX*, and *AKARI* (when available) provided the data for the infrared colors analysis of our objects. Optical and near-IR photometric data were corrected for extinction based on the $A_{V_{tot}}$ calculated in Sect. 3.2.2, adopting the A_I/A_V relations from Cardelli et al. (1989).

5.1. Optical colors

The spectral region represented by the $B - V$ vs. $U - B$ diagram is dominated by the photospheric radiation, which makes it very interesting to study the nature of the central source. The optical colors diagram is shown in Figure 5 displaying those of our objects that have available UBV magnitudes. For each object, two different pairs of colors are plotted according to the extinction correction explained in Sect. 3.2.2 (by adopting two luminosity classes). Superimposed to this distribution are plotted the theoretical curves for $\log g = 2, 3$, and 4, calculated by Bessel et al. (1998).

It is expected that H AeBes would have $\log g \approx 4$, similar to main sequence stars, whereas the post-AGB would have $\log g < 2$, typical of supergiants. However, as shown in Figure 5 the theoretical curves are clearly separated only for positive $B - V$ values, due to the presence of the Balmer discontinuity, which is

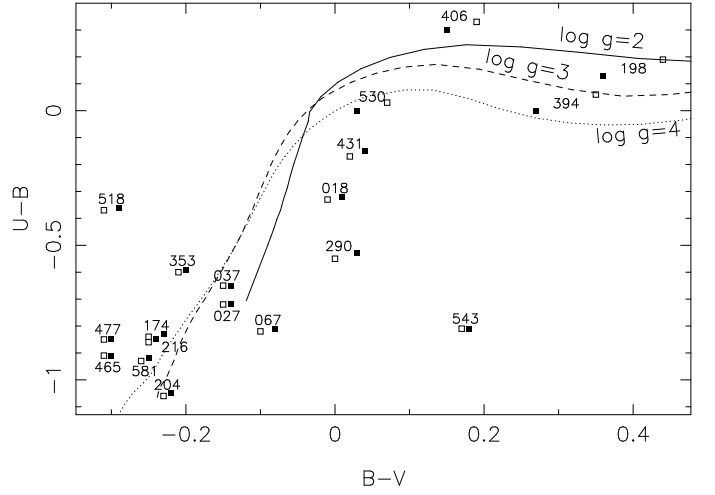


Fig. 5. Optical colors of the studied sample, after dereddening using different luminosity classes: main sequence (filled squares) and supergiants (open squares). The intrinsic colors from Bessel et al. (1998) are displayed for different surface gravities.

sensitive to surface gravity in this spectral range, being more significant for supergiants. In this case, only PDS406 seems to satisfy the gravity criterion. On the other hand, for $B - V \lesssim 0$, where part of our objects are located, the intrinsic colors from models for $\log g = 3$ and 4 are similar. In this case, we consider $U - B$ excess typical of evolved objects the values above the theoretical lines, as indicated for PDS465 and 581, the post-AGBs of our sample, as well as PDS174, 216, 353, 477, and 518.

5.2. Infrared colors

The IR colors probe the thermal emission from grains that can be originated from dust at different temperatures: (i) cold grains found in circumstellar shells at temperatures lower than 300K, or (ii) warm dust ($T \sim 1000K$) produced by a recent episode of mass loss in the case of post-AGBs, or from a protostellar disk in pre-MS stars.

5.2.1. Far-IR

Diagrams of IR colors have been used to identify post-AGB candidates according to their expected *locus* that is related to their evolution. Van der Veen & Habing (1988) suggested an evolutive sequence in a diagram of IRAS colors for post-AGB stars, defined by their mass-loss rate, in a scenario of short period Miras evolving into long period OH/IR stars. However, this hypothesis is based on observational results that are not firmly supported since the distances to OH/IR stars are uncertain (Whitelock et al. 1991). Other authors (e.g. Feast & Whitelock 1987) favor other scenario in which the Mira period is a function of its initial mass, where little changes in period or luminosity occur during the Mira evolution. This second scenario is supported by the results, obtained by Whitelock et al. (1991), on the evolution of Miras and the origin of their Period-Luminosity relationship.

García-Lario et al. (1997), hereafter GL97, analyzed a sample of post-AGBs comparing their position in the [12]-[25] vs. [25]-[60] diagram with several categories of objects, as for example: OH/IR variables (Sivagnanam 1989); pre-MS stars (Harris et al. 1988); and compact HII regions (Antonopoulos & Pottasch 1987).

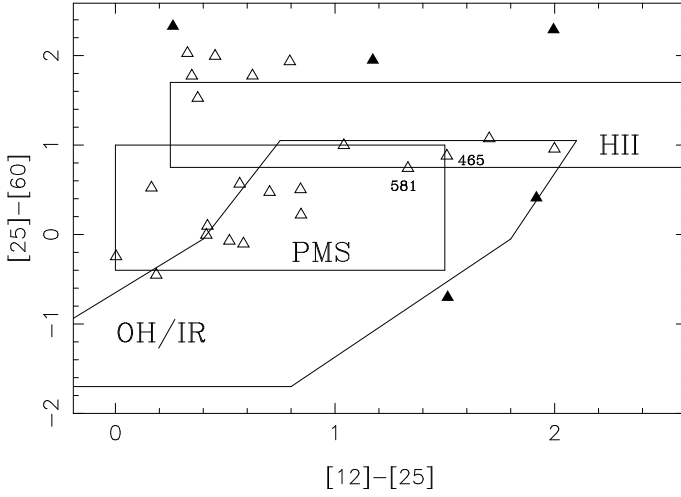


Fig. 6. Far-IR color-color diagram showing the regions for different categories of objects (GL97). Filled triangles are used to show the PDS sources with double peak in the SED, while open triangles represent single peak.

Figure 6 shows the distribution of our sample in the IRAS color-color diagram, with respect to the regions occupied by different classes of objects, as proposed by GL97. About 70% of our objects are located in the left part ($[12]-[25] < 1$) of this diagram, coinciding with the pre-MS box or above the HII region box ($[25]-[60] \geq 1.5$). Our remaining objects, among them PDS465 and 581, are found approximately in the right side of the diagram ($[12]-[25] \geq 1$). The $12 \mu\text{m}$ flux density distribution for IRAS sources located in this part of the diagram was studied by van der Veen et al. (1989, see region IV in their Figure 1). Based on the spatial distribution compared to the number of sources as a function of the $12 \mu\text{m}$ flux density, they proposed a separation of objects in this region of the IRAS colours diagram. According to van der Veen et al. (1989) young stars, which are associated to clouds, are those sources with $F_{12} < 2 \text{ Jy}$, while post-AGBs have $F_{12} > 2 \text{ Jy}$.

5.2.2. Mid-IR

The fluxes at 9, 18, 65, 90, 140, and $160 \mu\text{m}$ from the *AKARI* All Sky Survey (Ishihara et al. 2010) have been obtained for 78% of our sample. These data were used in the SED fitting discussed in Sect. 2.2. Following Ita et al. (2010) we verified the position of our sample in the $J - [18]$ vs. $[9] - [18]$ diagram, expressed in Vega magnitudes. In Figure 7, the *AKARI* colours of our sources are compared with the distribution of the *very likely* post-AGB stars from the Toruń Catalogue (Szczerba et al. 2007). The position of young objects is also displayed in this diagram, by plotting the YSOs from the *Spitzer* survey of young stellar clusters (Gutermuth et al. 2009) and the HAeBe stars from the Herbig & Bell Catalog (*HBC*, 1988). In spite of the better quality of the *AKARI* data, when compared to *IRAS* colours, the overlap of different categories also occurs in Figure 7, not distinguishing young objects nor evolved stars. Most of our sample is located in this overlap region, but three sources (PDS 204, 394, and 543) coincide with the region of post-AGBs, appearing more clearly separated, outside the main *locus* of the HAeBe stars, for example.

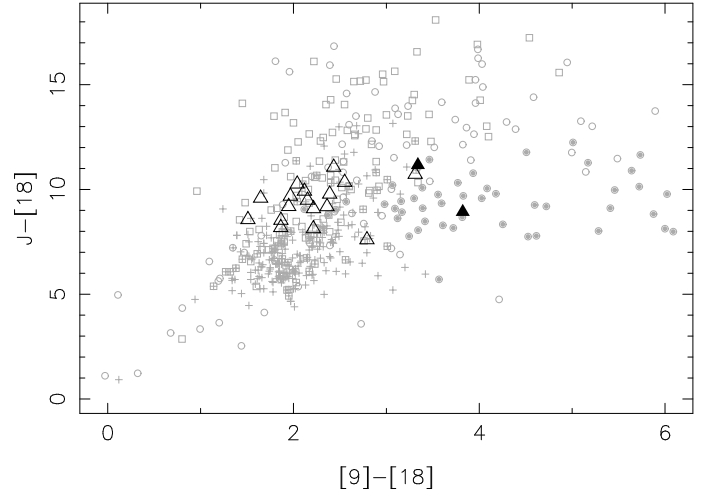


Fig. 7. Mid-IR color-color diagram based on *AKARI* fluxes. Triangles indicate our sample and grey circles represent the *very likely* post-AGBs from the Toruń Catalog. Filled symbols are used for objects having double peak in the SED, while open symbols represent single peak. The distribution of young objects is shown by grey squares (YSOs detected by *Spitzer*) and grey crosses (HAeBe stars from *HBC*).

5.2.3. Near-IR

Near-IR photometry can be used to check whether the main source of emission is photospheric, nebular or due to the presence of a circumstellar envelope. Figure 8 shows the $J-H$ vs. $H-K$ diagram studied by GL97 to compare AGB and post-AGB stars with different categories of objects, like YSOs (region III); main sequence (region I/II); T Tauri and HAeBe stars (region III/IV), and planetary nebulae. GL97 verified that about 2/3 of the planetary nebulae are found in the “nebulae box” (region V), defined by Whitelock (1985). The *very likely* post-AGB stars classified by Szczerba et al. (2007) are also plotted to illustrate the distribution of evolved objects with single or double peak in their SED.

Bessell & Brett (1988) studied the IR colours of Long-Period Variables (LPV), carbon stars and late-type supergiants. In Figure 8 we plot the schematic areas presented by Bessell & Brett (1988, Fig. A3), where carbon-rich stars are enclosed by dashed lines and oxygen-rich LPVs fall in the area defined by continuous line. The post-AGBs of our sample are located in region III from GL97, beyond the right-hand-end schematic area from Bessell & Brett. The only object coinciding with the region of carbon-rich stars is PDS551.

It can be noted in Figure 8 that several of our stars are found in the same region as post-AGBs having single peak SED, while our objects having double peak SED appear in region I. As mentioned in Sect. 1.2, Siódmiak et al. (2008) verified in near-IR diagrams a clear separation of nebulosity morphological classes SOLE and DUPLEX. The $J-H$ vs. $H-K$ diagram in Figure 8 shows the regions occupied by DUPLEX ($J-H > 1$) and SOLE (lower left side, $H-K < 0.75$). It is interesting to note that, in this diagram, the *locus* of the “stellar-like” objects dubbed by Siódmiak et al. (2008) (lower right side) coincides with the region IV, expected for TTs and HAeBe stars (GL97).

Comparisons of SED shapes are also interesting to be discussed on basis of near- to mid-IR excess, which is related to the morphology of circumstellar structure (Ueta et al. 2000, 2007). Figure 9 presents the $J-K$ vs. $K-[25]$ diagram where stellar-

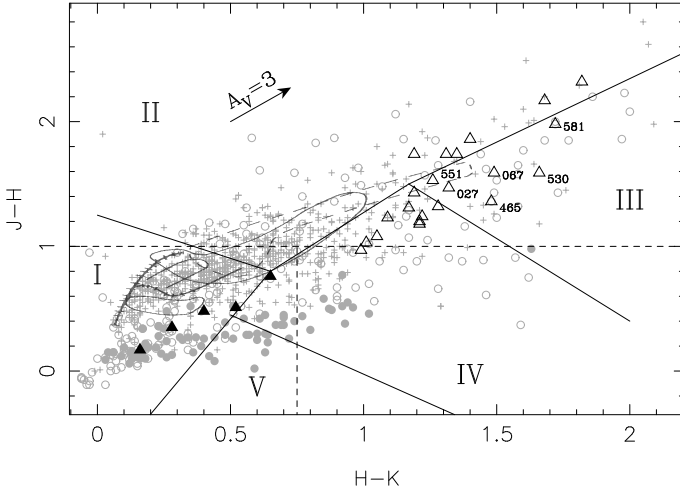


Fig. 8. Near-IR color-color diagram indicating the regions for different categories of objects defined by GL97 (separated by thin full lines), Siódmiak et al. (2008) (thin dashed lines), and Bessell & Brett (1988) (thick lines). Triangles are used to show our stars and grey circles represent *very likely* post-AGBs from the Toruń Catalog. Double peak SEDs are indicated by filled symbols (post-AGBs class IV). Grey crosses represent the H AeBe stars from *HBC*.

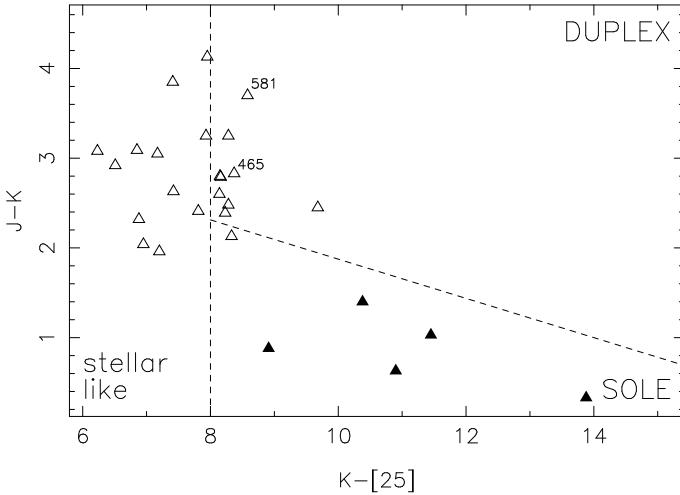


Fig. 9. Near- and mid-IR colors diagram indicating the regions defined by Siódmiak et al. (2008) (dashed lines). Filled triangles are used to show those of our stars with double peaked SEDs, while open triangles represent single peak SEDs.

like post-AGBs are in the left part ($K - [25] < 8$), while to the right are DUPLEXes (upper side) and SOLEs (lower part). Siódmiak et al. (2008) also correlate the SED shape with morphological groups: post-AGB class IV objects (double peak) are SOLE type, while classes I, II or III (single peak) are DUPLEX. As can be seen in Figure 9, the distribution of our double peak sources coincides with the SOLEs region. We consider these sources, as well as those located in the DUPLEX region, possible being post-AGB stars.

In spite of the good correlations between near-IR and SED shape, the discussion on elliptical or bipolar nebosity types is only tentative since the morphology is unknown for most of our objects. One exception is PDS204, for which Perrin et al. (2009) used IR imagery and polarimetric data to confirm the presence of an edge-on disk surrounded by an extensive envelope pierced

by bipolar outflow cavities. The results of the present work indicate that PDS204 has characteristics similar to post-AGBs, in particular its circumstellar morphology inferred from $J-K \times K-[25]$ colors, which is suggested to be DUPLEX (bipolar).

6. Discussion and Summary of Results

Aiming to analyse the similarities and differences between our sample of PDS sources and post-AGBs studied in other works, we have established several criteria to diagnose if the selected objects are pre-MS or not. The main result of this comparative study is the nomination of the likely post-AGB stars, indicated by notes in Table 2. For each given note, the adopted criteria and respective values that we consider typical characteristics of evolved objects are summarized as follows.

(a) The possible association with clouds was investigated by estimating the projected distance to the edge of the nearest cloud. According to the results presented in Sect. 3.1, note (a) indicates the objects having $d_{edge} > 0.5^\circ$.

(b) The circumstellar extinction, defined by f_{Av} , was estimated by subtracting interstellar extinction, obtained from Dobashi et al.'s A_V maps, of the total visual extinction, obtained from the $E(B - V)$ calculation. The fraction of source emission at $100\mu\text{m}$, defined by f_{F100} , was also evaluated in order to verify possible interstellar cirrus contamination. Note (b) indicates the objects showing $f_{Av} > 0.5$ and $f_{F100} > 0.5$, as described in Sect. 3.3.

(c) Our sample was also analyzed according to the spectral features, in particular the equivalent width of H_α line. In Figure 4 the strength of H_α is compared to the fractions of circumstellar emission f_{Sc} and f_{Av} . Note (c) indicates all the objects showing $W_{H\alpha} > 50 \text{ \AA}$ that have $f_{Sc} > 0.87$ and $f_{Av} > 0.5$.

(d) In Figure 5 (optical color-color diagram), seven objects have $U - B > -1$ and $B - V < -0.2$ that we consider indicative of $U - B$ excess typical of post-AGBs. As discussed in Sect. 5.1, no difference on gravities could be verified in the case of high temperatures, but one object with $B - V > 0.1$ seems to have low gravity, a possible indicator of evolved status.

(e) As mentioned in Sect. 5.2.1, the IRAS color-color diagram (Figure 6) shows eight of our objects with $[12]-[25] > 1$, all of them having $F_{12} > 2 \text{ Jy}$. This criterion has been suggested by van der Veen et al. (1989) to distinguish young stars, associated to clouds, from post-AGBs located in this part of the diagram that typically show $F_{12} > 2 \text{ Jy}$.

(f) and (g): The distribution of our sample in diagrams of near-IR colors was checked according the suggestion by GL97 that establishes different regions of these diagrams for each evolutive post-AGB phase. The objects located in regions I and III of Figure 8 are indicated by note (f). The diagram of near- and mid-IR colors shown in Figure 9 indicates that our objects having double peak SED are placed in the region of SOLE type post-AGBs and single peak sources coincide with DUPLEX objects, as suggested by Siódmiak et al. (2008). According the results discussed in Sect. 5.2.3, objects with $K-[25] > 8$ have note (g).

7. Conclusions and Perspectives for future works

The whole set of adopted criteria suggests that 26% (7/27 sources) of the studied sample are very likely post-AGB stars, which achieved five or more notes. Four objects having three or four notes are considered possible post-AGBs. As discussed below, PDS371 is also included in this list indicating that 18% (5/27) of the sample possibly are post-AGBs. Among the other objects having less than three notes, 8/27 sources (30% of the

Table 2. Parameters used in the sample analysis

PDS	f_{sc}	cloud	d_{edge} o	A_V mag	f_{Av}	$\langle F \rangle$ Jy	f_{F100}	Notes
018	0.90	L1647	1.79	1.3 ± 0.3	0.7	20 ± 2	0.7	a,b
027	0.96	L1659	5.60	1.2 ± 0.2	0.7	20 ± 3	0.7	a,b,c,f,g
037	0.93	FS134	-0.15	2.8 ± 0.4	0.4	156 ± 41	< 0.5	e,g
067	0.97	FS251	1.39	1.4 ± 0.3	0.7	300 ± 101	< 0.1	a,f
141	0.97	FS221	0.09	3.8 ± 0.8	0	14 ± 2	0.9	
168	0.75	L1536	-0.10	0.9 ± 0.6	0	14 ± 1	0.4	
174	0.97	L1616	0.07	1.2 ± 0.2	0.6	6 ± 4	1.0	b,c,d,e,g
193	0.70	L1641	-1.02	2.6 ± 0.6	0.4	37 ± 16	0.7	
198	0.85	L1641	-0.76	2.6 ± 0.6	0.3	37 ± 16	< 0.6	
204	0.95	L1570	5.91	0.9 ± 0.4	0.7	17 ± 1	0.9	a,b,c,e,g
207	0.89	L1557	-0.28	0.3 ± 0.5	0.9	16 ± 2	0.8	b,g
216	0.92	L1600	1.96	0.8 ± 0.2	0.8	18 ± 2	< 0.7	a,b,c,d,g
257	0.89	L1665	3.70	0.6 ± 0.1	0.8	21 ± 2	0.4	a
290	0.94	FS114	1.27	1.6 ± 0.2	0.2	37 ± 9	0.5	a,f,g
353	0.89	FS220	3.61	1.3 ± 0.2	0.6	80 ± 26	< 0.7	a,b,c,d,g
371	0.79	FS271	18.18	0.1 ± 0.1	1.0	5 ± 0	< 0.2	a
394	0.86	FS288	2.46	0.7 ± 0.2	0.5	49 ± 5	< 0.3	a,e,g
406	0.82	FS348	-0.20	1.2 ± 0.5	0	35 ± 5	0.2	d,g
431	0.94	FS372	1.42	1.6 ± 0.4	0	439 ± 155	< 0.8	a,c,f,g
465	0.92	L273	0.58	0.6 ± 0.2	0.8	30 ± 3	0.7	a,b,c,d,e,f,g
477	0.87	L318	0.10	2.6 ± 0.4	0.4	120 ± 14	0.2	d
518	0.91	L511	0.09	5.4 ± 1.0	0.2	105 ± 11	0.9	d
520	0.84	L571	0.49	5.5 ± 0.8	0	79 ± 26	< 0.1	
530	0.82	L637	0	1.0 ± 0.3	0.3	38 ± 5	0.3	f
543	0.94	L621	-3.01	4.6 ± 0.6	0.2	164 ± 47	0.2	e,f,g
551	0.96	L628	0.30	6.3 ± 0.7	0	196 ± 43	< 0.5	f,g
581	0.94	L813	1.28	0 ± 0.1	1.0	21 ± 3	0.8	a,b,c,d,e,f,g

Columns description: (1) PDS name; (2) fraction of circumstellar luminosity; (3, 4) nearest cloud and respective distance to the edge; (5) visual extinction from Dobashi et al. (2005); (6) “net” visual extinction; (7,8) background mean flux and fraction of source emission at $100\mu\text{m}$.

Notes: (a) $d_{edge} > 0.5^\circ$; (b) $f_{Av} > 0.5$ and $f_{F100} > 0.5$; (c) high values of $W_{H\alpha}$, f_{Av} and f_{F100} ; (d) U-B excess; (e) $[12]-[25] > 1$ and $F_{12} > 2$ Jy; near-IR colors typical of post-AGB: (f) J-H and H-K, (g) J-K and K-[25].

sample) are unlikely post-AGB since they were confirmed in the literature as pre-MS stars. The nature of the remaining 7/27 objects is unclear. Individual comments are given in Appendix A to present recent results from literature related to the nature of our stars.

PDS465 and 581 are well known post-AGBs. The other very likely post-AGBs indicated by us are PDS 27, 174, 204, 216, and 353. Results from other works support these suggestions at least for two of them: PDS 27 (Suárez et al. 2006) and PDS 174 (Sunada et al. 2007).

The unlikely post-AGB objects: PDS 18, 37, 141, 168, 193, 198, 406, and 518 are confirmed pre-MS stars (see Appendix A). Other sources with less than three notes are: PDS 67, 207, 257, 477, 520, 530, and 551, which were not previously studied in the literature.

Other objects whose nature remains to be confirmed are PDS 290, 394, 431, 543 that we suggest to be possible post-AGB objects. As discussed in Section 4, PDS371 is included in this group since it shows spectral features similar to proto-PN. The *AKARI* colours, discussed in Sect. 5.2.2, were not used to nominate the post-AGBs, due to the position of our sample, mainly concentrated in the region of overlap of young and evolved objects in Figure 7. However, it is interesting to note that three sources appear out of this overlap region. Indeed, PDS 204 (very likely post-AGB), and PDS 394 and 543 (possible post-AGBs) have colours $[9]-[18] > 3$ mag, which coincide with the *locus* of most of the post-AGB class IV, confirming the classification that we suggest for these PDS sources.

We are aware that additional observations are needed to definitively classify the candidates, as mentioned by Szczerba et al. (2007) in their evolutive catalogue of post-AGB objects. Several techniques and instruments operating in different spec-

tral domains can be used to confirm the evolved nature of our candidates. Detailed spectroscopic analysis is required to obtain a better determination of spectral type and luminosity class that could be evaluated through the spectral lines sensitive to changes in gravity (Pereira & Miranda 2007). Spectral synthesis, for example, would provide abundances of C and O, whose ratio is used in the classification of post-AGB stars (van der Veen et al. 1989). Abundances of Ba and Sr are also interesting to be determined, since the enrichment of elements produced by s-process is expected to occur during the post-AGB phase (Parthasarathy 2000). However, a detailed spectral analysis of absorption lines is constrained to objects with intermediary to low T_{eff} , which is not the case of our sources that do not show these spectral features. It is more indicated, in this case, to study the emission line profile of He I λ 5876, or the strength of [N II] λ 5754 relative to [O I] λ 6302, that were used by Pereira et al. (2008), for example, to indicate the nature of a proto-PN candidate. Evidence of a carbon-rich chemistry can be also obtained through mid-infrared spectroscopy from 10 to $36\mu\text{m}$, as the example of the study by Hrivnak et al. (2009).

Direct imagery remains the most interesting tool to reveal the morphology of the nebulae. Our sources show several indications of having a considerable amount of circumstellar material that could be detected in high resolution images. Ueta et al. (2007), for example, studied the post-AGB circumstellar structures via dust-scattered linearly polarized starlight, by using imaging-polarimetric data obtained with NICMOS/HST. It would be very interesting to develop a SED fitting based on more reliable circumstellar parameters and a disk model more realistic than that adopted in the present work. We intend to apply a radiative transfer model specifically developed to study the physical conditions like mass loss and envelope density of the post-AGB.

Our results indicate new likely and possible post-AGBs that open promising and exciting perspectives to continue studying these targets.

Acknowledgements. RGV and JGH thank support from FAPESP (Proc. No. 2008/01533-4; Proc. No. 2005/00397-1). This research has made use of the SIMBAD database, operated at CDS, Strasbourg, France.

References

- Acke, B., & Van den Ancker, M. E., 2006, A&A, 457, 171
- Acke, B., Verhoelst, T., Van den Ancker, M.E. et al., 2008, A&A, 485, 209
- Acke, B., Bouwman, J., Juhász, A., et al. 2010, ApJ, 718, 558
- Adams, F. C. & Shu, F. H., 1986, ApJ, 308, 836
- Alcalá, J. M., Spezzi, L., Chapman, N., Evans II, N. J. et al., 2008, ApJ, 676, 427
- Alecian, E., Catala, C., Wade, G. A., Donati, J.-F., Petit, P., et al. 2008, MNRAS, 385, 391
- Alonso-Albi, T., Fuente, A., Bachiller, R., et al., 2009, A&A, 497, 117
- Andrews, S. M., & Williams, J. P., 2005, ApJ, 631, 1134
- Antonopoulos, E., & Pottasch, S. R. 1987, A&A, 173, 108
- Bessel, M. S., Brett, J.M., 1988 PASP, 100, 1134
- Bessel, M. S., Castelli, F., & Plez, B. 1998, A&A, 333, 231
- Beskronnaya, N. G., Pogodin, M. A., Najdenov, I. D., & Romanyuk, I. I., 1995, A&A, 298, 585
- Bitner, M. A., Richter, M. J., Lacy, J. H. et al., 2008, ApJ, 688, 1326
- Bowers, P. F., & Knapp, G. R. 1989, ApJ, 347, 325
- Brand, J., Blitz, L., Wouterloot, J. G. A., Kerr, F. J. 1987, A&A 68,1
- Cardelli, J. A., Cleyton, G. C., & Mathis, J. S. 1989, ApJ, 345, 245
- Carpenter, J. M., Bouwman, J., Silverstone, M. D. et al., 2008, ApJS, 179, 423
- Catala, C., Donati, J. F., Böhm, T.; Landstreet, J.; Henrichs, H. F., et al., 1999, A&A, 345, 884
- Connelley, M. S., Reipurth, B., Tokunaga, A. T., 2007, AJ, 133, 1528
- Connelley, M. S., Reipurth, B., Tokunaga, A. T., 2008, AJ, 135, 2496
- de Jager, C., & Nieuwenhuijzen, H., 1987, A&A, 177, 217
- De Marco, O., 2009, PASP, 121, 316
- Dennis, T. J., Cunningham, A. J., Frank, A. et al 2008, ApJ, 679, 1327
- Dobashi, K., Uehara, H., Kandori, R., Sakurai, T., Kaiden, M., et al., 2005, PASJ, 57, SP1
- Epchtein, N., Le Bertre, T., & Lépine, J.R.D., 1990, A&A, 227, 82
- Evans, N. J., Dunham, M. M., Jorgensen J.K. et al., 2009, ApJS, 181, 321
- Feitzinger, J. V., & Stüwe, J. A. 1984, A&AS, 58, 365
- Feast, M. W., Whitelock, P. A., 1987 In: *Late Stages of Stellar Evolution*, p. 33, eds. Kwok, S. & Pottasch, S. R., Reidel, Dordrecht
- Froebrich, D., 2005, ApJS, 156, 169
- Furlan, E., McClure, M., Calvet, N. et al. 2008, ApJS, 176, 184
- García-Lario, P., Manchado, P., Pych, W., & Pottasch, S.R. 1997, A&AS, 126, 479
- Gregorio-Hetem, J., Lépine, J. R. D., Quast, G. R., Torres, C. A. O., & de la Reza, R. 1992, AJ, 103, 549
- Gregorio-Hetem, J., & Hetem, A. Jr. 2002, MNRAS, 336, 197
- Goto, M., Henning, Th., Kouchi, A. et al., 2009, ApJ, 693, 610
- Gutermuth, R. A., Megeath, S. T., Myers, P. C., Allen, L. E., Pipher, J. L., Fazio, G. G., 2009, ApJS 184, 18G
- Harris, S., Clegg, P., & Hughes, J. 1988, MNRAS, 235, 441
- Herbig, G. H., Bell, K. Robbin 1988, Third Catalog of Emission-Line Stars of the Orion Population, Lick Observatory Bulletin, No. 1111
- Herbig, G., Vacca, W. D., 2008, AJ, 136, 1995
- Hillenbrand, L. A., Strom, S. E., Vrba, F. J., & Keene, J. 1992, ApJ, 397, 613
- Hrivnak, B.J., Volk, K., & Kwok, S., 2009, ApJ, 694, 1147
- Ishihara, D., Onaka, T., Katata, H., et al., 2010 A&A 514A, II
- Ita, Y., Matsuura, M., Ishihara, et al., 2010, A&A 514A, 2I
- Jablonski, F., Baptista, R., Barroso, F., Jr., Gneiding, C., Rodrigues, F., & Campos, R. P. 1994, PASP, 106, 1172
- Kawamura, A., Onishi, T., Yonekura, Y. et al., 1998, ApJS, 117, 387
- Lee, C. -F., Hsu, M. -C., Sahai, R., 2009, ApJ, 696, 1630
- Liu, W. M., Hinz, P. M., Meyer, M. R. et al., 2007, ApJ, 658, 1164
- Luhman, K. L., Whitney, B. A., Meade, M.R. et al., 2006, ApJ, 647, 1180
- Luna, R., Cox, N. L. J., Satorre, M. A. et al., 2008, A&A, 480, 133
- Lynds, B. T. 1962, ApJS, 7, 1
- Magakian, T. Y., 2003, A&A, 399, 141
- Malfait, K., Bogaert, E., & Waelkens, C. 1998, A&A, 331, 211
- Meeus, G., Waters, L. B. F. M., Bouwman, J., van den Ancker, M. E., Waelkens, C., & Malfait K. 2001, A&A, 365, 476
- Montez, R., Kastner, J. H., Balick, B., Frank, A., 2009, ApJ, 694, 1481
- Mottram, J. C., Hoare, M. G., Lumsden, S. L. et al., 2007, A&A, 476, 1019
- Otrupcek, R. E., Hartley, M., Wang, J.-S., 2000, PASA, 17, 92
- Parthasarathy, M., 2000, IAUS, 177, 225
- Pereira, C. B., & Miranda, L. F., 2005, A&A, 433, 579
- Pereira, C. B., & Miranda, L. F., 2007, A&A, 462, 231
- Pereira, C. B., Marcolino, W. L. F., Machado, M., & de Araújo, F. X., 2008, A&A, 477, 877
- Perrin, M. D., Vacca, W. D., Graham, J. R., 2009, AJ, 137, 4468
- Pestalozzi, M. R., Minier, V., Booth, R. S., 2005, A&A, 432, 737
- Porras, A., Jorgensen, J. K., Allen, L. E. et al., 2007, ApJ, 656, 493
- Raga, A. C., Riera, A., Mellema G. et al., 2008, A&A, 489, 1141
- Riera, A., García-Lario, P., Manchado, A., Potash, S. R., & Raga, A. C. 1995, A&A 302, 137
- Reed, B. C., 2005, AJ, 130, 1652
- Rodrigues, C. V., Jablonski, F. J., Gregorio-Hetem, J., Hickel, G. R., & Sartori, M. J., 2003, ApJ, 587, 312
- Rodrigues, C. V., Sartori, M. J., Gregorio-Hetem, J., & Magalhães, A. M., 2009, ApJ, 698, 2031
- Rowan-Robinson, M., 1986, MNRAS, 219, 737
- Sanchez Contreras, C., Sahai, R., Gil de Paz, A., Goodrich, R., 2008, ApJS, 179, 166
- Sartori, M. J., Gregorio-Hetem, J., Rodrigues, C. V., Hetem, A., Batalha, C. 2010, AJ, 139, 27
- Savage, B. D., & Mathis, J. S. 1979, ARA&A, 17, 73
- Schultz, G. V., & Wiemer, W. 1975, A&A, 43, 133
- Siódmiak, N., Meixner, M., Ueta, T., Sugerman, B. E. K., Van de Steene, G. C., Szczerba, R., 2008, ApJ, 677, 382
- Sivagnaman, P. 1989, PhD Thesis, University of Paris VII, France
- Smolders, K., Acke, B., Verhoelst, T. et al. 2010, A&A, 514, L1
- Steffen, M., Szczerba, R., Schnberger, D. 1998, A&A, 337, 149
- Steffen, W., Garcia-Segura, G., Koning, N., 2009, ApJ, 691, 696
- Straizys, V., & Kuriliene, G. 1981, Ap&SS, 80, 353
- Strom, S. E., Strom, K. M., & Grasdalen, G. L., 1975, ARA&A, 13, 187
- Suárez, O., García-Lario, P., Manchado, P., Manteiga, Ulla, Pottasch, S.R., 2006, A&A, 458, 173
- Suárez, O., Gómez, J. F., Morata, O., 2007, A&A, 467, 1085
- Sunada, K., Nakazato, T., Ikeda, N. et al., 2007, PASJ, 59, 1185
- Szczerba, R., Siódmiak, N., Stasińska, G., Borkowski, J., 2007, A&A, 469, 799
- Terebey, S., Fich, M., Noriega-Crespo, A., 2009, ApJ, 696, 1918
- Torres, C. A. O., Quast, G. R., de la Reza, R., Gregorio-Hetem, J., & Lépine, J. R. D. 1995, AJ, 109, 2146
- Torres, C. A. O. 1999, Publication of CNPq/Observatório Nacional (Brazil), 10, 1
- Ueta, T., Meixner, M., & Bobrowsky, M. 2000, ApJ, 528, 861
- Ueta, T., Murakawa, K., & Meixner, M., 2007, AJ, 133, 1345
- Urquhart, J. S., Busfield, A. L., Hoare, M. G. et al., 2007, A&A, 474, 891
- Urquhart, J. S., Busfield, A. L., Hoare, M. G. et al., 2008, A&A, 487, 253
- Van den Ancker, M., 1999, PhD Thesis, University of Amsterdam
- Van der Veen, W. E. C. J., & Habing, H. J., 1988, A&A, 194, 125
- Van der Veen, W. E. C. J., Habing, H. J., Geballe, T. R., 1989, A&A, 226, 108
- Vieira, S. L. A., Corradi, W. J. B., Alencar, S. H. P., Mendes, L. T. S., Torres, C. A. O., Quast, G. R., Guimarães, M. M., & da Silva, L. 2003, AJ, 126, 2971
- Winkel, H. V. 2003, ARA&A, 41, 391
- White, R. J. & Hillenbrand, L. A., 2004, ApJ, 616, 998
- Whitelock, P. A. 1985, MNRAS, 237, 479
- Whitelock, P. A., Feast, M., Catchpole, R., 1991, MNRAS, 248, 276.
- Ybarra, J. E. & Lada, E. A., 2009 ApJ, 695L, 120

Appendix A: Individual Comments

The literature has been searched for results confirming the nature of the studied objects, which are found for 15/27 of the sample, all of them consistent with the results of the present work. In this section we separate these references in three parts: (i) previously known young stars; (ii) very likely post-AGBs; (iii) possible post-AGB or pre-MS.

A.1. Young stars

PDS18 is included in the study of YSOs showing IR nebula, presented by Conneley et al. (2007). A reflection nebulae associated to PDS18 is catalogued by Magakian (2003). Additionally, Conneley et al. (2008) also verified the presence of an arc-shaped nebula (~ 8 arcsec to the northeast) around this object.

PDS141 (DK Cha), one of the most studied object of our sample, is a Class I pre-MS star. Results based on *Spitzer* data

have been presented by Porras et al. (2007), Alcalá et al. (2008), Ybarra & Lada (2009), Evans et al. (2009), for example. The disk structure was studied by Liu et al. (2007). CO emission has been reported by Otrupcek et al. (2000).

Spitzer data are also provided for **PDS168** (Luhman et al. 2006, Furlan et al. 2008), which is considered a Class I protostar (White & Hillenbrand 2004, Terebey et al. 2009). The protoplanetary disk was studied from H₂ emission (Bitner et al. 2008) and from millimeter data (Andrews & Williams 2005).

PDS193 is in the 3 μ m spectroscopic survey of HAeBes, presented by Acke & van den Ancker (2006). **PDS406** was included in the study of Class 0 protostars by Froebrich (2005) and appears in the reflection nebulae catalogue from Magakian (2003).

Sunada et al. (2007) included **PDS198** in their study of H₂O maser, but no maser emission was found for this object, probably due to its intermediate-mass (F0 type star). Acke & van den Ancker (2006) consider PDS198 as HAeBe.

PDS518 is also a well studied young B star (Acke et al. 2008), for which 3 μ m spectroscopy of protoplanetary disks is presented by Goto et al. (2009); the circumstellar structure was also studied by Alonso-Albi et al. (2009). Conneley et al. (2008) included PDS518 in a study of multiplicity of embedded protostars.

A.2. Post-AGB

PDS27 appears in the list of Suárez et al. (2006) who presented a Spectroscopic Atlas of post-AGB stars. CO emission has been reported by Urquhart et al. (2007).

The emission of H₂O maser (usually found in massive protostars) was not detected in the survey by Sunada et al. (2007) in the case of **PDS174** that is a result consistent with our suggestion of post-AGB candidate for this object.

As stated before, PDS465 and PDS581 are confirmed post-AGB objects largely studied in the literature. The most recent results for **PDS465** are presented by Lee et al. (2009), De Marco (2009), Luna et al. (2008), Raga et al. (2008), among others, and for **PDS 581**: Steffen et al. (2009), Montez et al. (2009), Dennis et al. (2008), Sanchez Contreras et al. (2008), for example. CO emission associated to PDS581 has been reported by Urquhart et al. (2008). Both objects are listed in the Toruñ Catalogue, classified by Szczerba et al. (2007) as *IRAS* selected source (PDS465) or reflection nebulosity (PDS581).

PDS 394 is studied as post-AGB candidate by Suárez et al. (2006) and Szczerba et al. (2007).

PDS204 (MWC778) is considered a peculiar object in the H₂O maser study of post-AGB (Suárez et al. 2007, 2006). CO emission has been reported by Kawamura et al. (1998) and Urquhart et al. (2007). Herbig & Vacca (2008) suggested that MWC778 has a SED slope of pre-MS embedded object, which has spectral type F or G, due to the presence of metallic absorption lines. From IR imagery and polarimetric data, Perrin et al. (2009) confirm the presence of an edge-on disk surrounded by an extensive envelope pierced by bipolar outflow cavities. They argue that MWC778 has high bolometric luminosity inconsistent with F or G type star. The results of the present work indicate that PDS204 has characteristics similar to post-AGBs, in particular its circumstellar morphology inferred from J-K \times K-[25] colors, which are found in DUPLEX (bipolar) post-AGBs.

PDS216 has been included in the study of hydrocarbon molecules in Herbig Ae stars (Acke et al. 2010) aiming to verify the correlation of effective temperature with the 7.8 μ m feature, when comparing their sample with low- and high-mass stars. Considering that similar results are also found for S-type AGB

stars (Smolders et al. 2010), Acke et al. (2010) conclude that the chemistry of hydrocarbon molecules in the circumstellar environment is mainly affected by stellar radiation field regardless of the evolutionary status.

A.3. Possible post-AGB or pre-MS

PDS37 is in the list of post-AGB stars studied by Szczerba et al. (2007), but it is considered YSO in the work of Mottran et al. (2007) and in the *Spitzer* mid-IR survey by Carpenter et al. (2008). CO emission has been reported by Urquhart et al. (2007).

PDS371 has been included in the photometry and spectroscopy for luminous stars catalogue by Reed (2005). However, no additional information is available than those given by the PDS Catalogue (Vieira et al. 2003).

CO emission has been reported by Brand et al. (1987) for PDS290 and PDS353.

Pestalozzi et al. (2005) detected in **PDS431** methanol maser emission, which usually is considered an indicator of massive star formation as well as observed in Class 0 protostars. CO emission has been reported by Urquhart et al. (2007).